OPEN ACCESS

# Fully Printed pH Sensor based on Polyaniline/Graphite Nanocomposites

*Journal of The Electrochemical Society*, 2023 **170** 027501

# Fully Printed pH Sensor based on Polyaniline/Graphite Nanocomposites

**Shirin Mahinnezhad, Ricardo Izquierdo, and Andy Shih**[z]

*Department of Electrical Engineering, École de technologie supérieure, Montreal, Quebec, Canada*

Recently, there is an exceptional growth in research related to the development of flexible sensors for health analysis. pH measurements can be done non-invasively and continuously, making it an excellent parameter for monitoring different stages of wound healing. Here, we report pH functionality of a polyaniline/graphite (PANI/G) composite in a fully-printed potentiometric pH sensor and the effect of graphite loading on sensor functionality. PANI/G composites in different ratios were aerosol-jet printed on Ag/AgCl with and without a graphite layer as the working electrode in a two-electrode potentiometric sensor on a flexible substrate. The role of graphite layer on working electrode in functionality of the sensor has been investigated. The PANI/G composites were prepared by a solution processing method using a graphite paste and polyaniline emeraldine salt powder. Samples were characterized by XRD, SEM, and FTIR analysis to investigate the relations between the physical and chemical relations and the performance of the sensors. The sensors were tested in the pH range from 3 to 10, exhibiting a linear, stable and near-Nernstian sensitivity of 53 mV $pH^{-1}$ and a response time of 15 s.

 [DOI: 10.1149/1945-7111/acb5c3]

Manuscript submitted September 30, 2022; revised manuscript received January 14, 2023. Published February 6, 2023.

pH sensors are vital analytical tools in clinics, laboratories and different industries which provides a logarithmic measure of hydrogen ion concentration for assessing human health as well as water and food quality.[1] Important challenges in which the technology faces are its lack of flexible form factor and wearability needed for integration with smart health monitoring systems such as smart bandages and IoT devices.[2,3] There is also a need for miniaturized pH sensors with good sensitivity, good stability and fast response times to enable real time monitoring as well as high accuracy for physiological measurements.[4–7] Sensors based on conducting polymers have the advantages of mechanical flexibility, high electrical conductivity, simplicity, and low-cost.[8] Polymers with $\pi$-conjugated double bonds in the chain have properties like low ionization potential, high electron affinity and low energy electronic transitions. These properties make polymers easily and quickly oxidized and reduced, with their functional groups being protonated and deprotonated at different pH levels.[9] Wang et al. described different methods for fabrication of polyaniline-based wearable pH sensors which have good functionality in the physiological range, working on the basis of the Nernstian equation.[10]

Polymer and carbon composites are one of the most attractive sensing materials because of their considerable flexibility, simplicity and low-cost.[11–16] For example, polyaniline (PANI) has been used in various printed and flexible sensors as it is easy to synthesize by electrochemical, chemical and oxidative polymerization methods and exhibits adjustable electrical conductivity.[17–19] PANI's behavior to pH variation is promising due to its fast response time when exposed to acidic solutions (protonation), becoming a more conductive emeraldine salt form, and when exposed to alkaline solutions (deprotonation), forming a more insulating emeraldine base.[20] This versatile behavior enables a controllable conductivity in the polyaniline chain that depends on the protonation degree.[21] Furthermore, PANI's affinity for reversible pH sensing is suitable for the stabilization of enzymes, ligands and antibodies, making PANI useful for new flexible and wearable biological sensors.[10,22–30]

The PANI-based potentiometric pH sensor sensing mechanism is based on the redox equilibrium between $H_3O^+$ and PANI phase transitions.[31–33] According to Nernst equation, the sensitivity in potentiometric pH sensors can be obtained by the slope of the linear regression:[34]

$$E = E_0 - (2.303\,RT/F)pH = E_0 - 0.05916\,pH \quad [1]$$

where $E_0$ is the standard electrode potential, T is the temperature, R is the gas constant, and F is Faraday's constant. Based on the Nernst equation, the maximum theoretical sensitivity is $-59$ mV $pH^{-1}$ at room temperature.

Polyaniline can be blended with various polymers such as polyethylene, polyvinyl chloride, polystyrene and thermoplastic elastomers to achieve conductive composites with fine-tuned electrical conductivity.[20] Polyaniline is also a good candidate to be used with inorganic materials such as metal oxides for different sensing applications. For example, PANI-$TiO_2$ composites were formed as thin films, exhibiting a porous nanostructure, which is desired for gas sensing.[35] Another example of PANI sensor fabrication is the use of polyaniline nanofibers in a silica sol just prior to gelation which led to increased electrically conductivity and flexural strength of the composite and which has applications in hydrochloric acid and ammonia gas molecule detection.[36]

Most importantly, PANI can be synthesized and combined with different carbon-based materials such as carbon black (CB), graphite (G), graphene (Gr), exfoliated graphite (EG), and graphene oxide (GO).[37] In particular, graphite has desirable metallic and nonmetallic characteristics such as low electrical conductivity and high thermal resistance. These properties enable graphite to be implemented in various applications such as fuel cells, batteries, printed sensors, and refractories.[38,39] Different polymerization methods of PANI and its use with graphite have been reported such as the emulsion polymerization technique to improve PANI properties with exfoliated graphite nanoplatelets and expended graphite which led to an improvement in electrical conductivity, thermal energy storage capacity, and thermal conductivity.[20,40,41] Monomer aniline is typically used in many of the electropolymerization methods and has been doped with different materials including graphite.[20] However, electropolymerization of PANI does not lend itself to a fully printed process which would be required for large scale production. In past studies on polyaniline/graphite (PANI/G) composites, the role of graphite on enhancing the conductivity of these composites has been investigated and these PANI/G composites show controllable conductivities as a function of pH.[42]

In this research, we forego the direct polymerization method, which is not suitable for cost-effective mass production, and instead prepare a polyaniline/graphite (PANI/G) composite dispersion with N-methyl pyrrolidone (NMP) solvent to be used in the printing of pH potentiometric sensors. Both PANI and graphite possess good electrical conductivity and thermal stability. The surface

[z]E-mail: andy.shih@etsmtl.ca

morphology, structural, and electrical properties of the composites and their effect on the performance of the sensors have been investigated and presented.

## Experimental

***Reagents and solutions.—***The PANI-emeraldine salt (PANI-ES) powder (Mw >15,000), NMP solvent and buffer solutions were acquired from Sigma Aldrich and the Ag/AgCl paste was purchased from Sun Chemical. The commercial graphite paste and the dielectric passivation paste was bought from DuPont.

***Apparatus.—***The pH values of buffered solution were adjusted by adding HCl or NaOH solution to standard buffer solutions (Cole Parmer). In order to control the accuracy of the measurements, the pH values were regularly validated by a commercial pH meter (Accumet AB 15/15 + bench-top meter). The potentiometry voltage-time (V–t) measurements were carried out with the help of an Agilent 34401-A device.

***Sensor design and fabrication process.—***Here, PANI-ES powder dispersed in NMP was used along with the commercial graphite paste to modify the working electrode and investigate the role of graphite both printed on Ag/AgCl electrode to be modified by the active composites and also in composites to see how the interaction between PANI chain and graphite active sites can improve the sensitivity and stability of the sensors.

Active composites were prepared by solution processing method to avoid the potentially toxic by-products from the electropolymerization process of PANI. Three composites of polyaniline and graphite have been tested to obtain the optimal sensor characteristics in terms of pH sensitivity, stability, and physical properties.

pH sensors were designed with two electrodes, an active layer and a dielectric passivation layer deposited on top of each other over a pre-cleaned PET substrate. The electrodes were printed with Ag/AgCl paste as the first layer and dried in an oven at 120 °C for 1 h. An optional graphite layer was screen-printed in a circular pattern over one of the Ag/AgCl electrodes to act as the base for the working electrode (WE) and was dried at 120 °C for 30 min. Then, PANI/G composites were aerosol-jet printed on the surface of the Ag/AgCl or G/Ag/AgCl WE. The surface morphology of the active layer on both graphite layer and Ag/AgCl electrode was studied using high resolution scanning electron microscope (SEM, Hitachi SU-8230), and the thickness of the electrodes was measured by profilometry (Bruker Dektak XT, USA). In Fig. 1b, the SEM image of the WE show the attachment of PANI chain on the graphite surface. Finally, a dielectric paste was screen-printed on the electrodes to electrically isolate the contacts from the test solution and dried at 120 °C for 1 h. The sensor dimensions were 13.5 mm length × 8 mm width × 20 $\mu$m thick, shown in Fig. 1b. PANI/G composites were deposited on the working electrodes with and without screen-printed graphite layer on top of the Ag/AgCl electrode using aerosol-jet printing and changes in sensitivity and stability of the sensors were investigated.

***Active materials preparation.—***Active materials were prepared by a solution processing method with PANI-ES powder being dissolved in NMP solvent at a concentration of 10 mg $ml^{-1}$. The dispersion was stirred at room temperature for 20 min at 500 RPM. PANI/G composites were then prepared with different wt% of graphite by mixing graphite paste with PANI/NMP solution. The samples are listed in Table I.

## Results and Discussion

***Characterizations.— SEM.***—The surface morphology of PANI/G composites with different graphite concentration was analyzed using a scanning electron microscope (SEM, model Hitachi SU-8230).

The SEM micrographs of PANI/G composites at different ratios are presented in Fig. 2, showing the attachment of PANI chains on

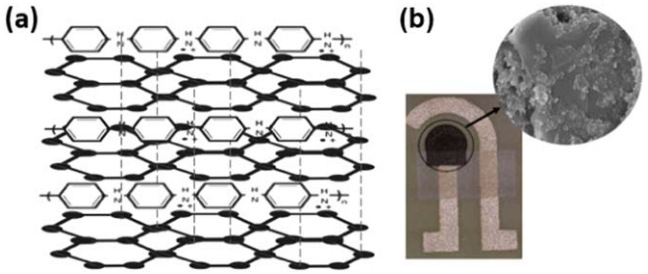


**Figure 1.** (a) Schematic illustration of the doped form of polyaniline chain and the graphite layers interaction. (b) Top-view optical micrograph of the potentiometric pH sensor and SEM mage of the aerosol-jet printed working electrode.

the graphite active sites as well as the graphite being dispersed uniformly in the PANI matrix. It was shown that a large number of PANI covered a small amount of graphite, resulting in flake-like particles. Similar observation was reported by Ju-Lan Zeng and coworkers which emphasized the use of exfoliated graphite nanoplatelets in PANI.[27,30] However, PANI interaction is only on the exposed layer of the graphite surface which is due to the small interspace of the graphite interlayer.

PANI/G composite solutions printed directly on the Ag/AgCl electrode without the graphite layer is also shown in Figs. 2e–2f. The PANI/G composite formed a uniform layer on top of the Ag/AgCl film but there is no visible interaction between PANI chain and Ag/AgCl film as it doesn't have the desired porous morphology and the active sites for potential attachment of PANI chain. In previous reports in which synthesis of PANI/Ag/AgCl nanocomposites was performed, the possible mechanism of the formation of the nanocomposites depended on the synthesis process.[43] The molar ratio of Ag to $Cl^-$ turned out to be important as unreacted $Ag^+$ serves as the oxidant for the polymerization of aniline. Thus, interactions between polyaniline and Ag/AgCl cannot be obtain by printing the PANI solution directly on top of Ag/AgCl film.[43]

*Fourier transform infrared spectra analysis.*—The structural changes in the different PANI/G composites have been observed through FTIR spectra, shown in Fig. 3. The PANI-ES has functional bonding characteristics in the range wavenumber of 400–3000 $cm^{-1}$. The bonding characteristics formed between 1440–1700 $cm^{-1}$ show the presence of stretched C=C bond of quinoid and benzenoid rings at 1663 and 1505.8 $cm^{-1}$, respectively. These matches previous reports of characteristic PANI peaks at 1600 $cm^{-1}$ and 1497 $cm^{-1}$.[44] The peak at 1293.7 $cm^{-1}$ shows the presence of –-N bonds or quinoid rings. This quinoid ring wavenumber indicates the existence of $\pi$ electron delocalization which appear through protonation process of polyaniline chain. The C–H in-plane out-of-plane bending vibrations are shown at 1068.7 and 1026 $cm^{-1}$.[45] Also, the PANI-ES peaks at 1263.2, 1108.2, and 747 $cm^{-1}$ correspond to the C–N stretching, C=N stretching, and 1,4-substituted phenyl ring stretching, respectively.[31,42] There is a shift of peaks and increase of intensities due to interlayer bonding between graphite and PANI. The 1461 $cm^{-1}$ peak corresponds to the C–N stretching vibration which indicates the polaron structure, where PANI in doped state was proven.[42] The polaron structure leads to energy bands overlapping between the valence and conduction bands, resulting in an increase in conductivity by several orders of magnitude.[31,46,47] Polyaniline chains were attached to the graphite plane resulting for more electron delocalization. Intensities of PANI/G are different at different graphite ratio of graphite and this is due to the N–H bonding in polyaniline and hydroxyl group in graphite. The PANI/G composites intensities increased as the graphite content increased. The intercalation between PANI and graphite would weaken the N–H bonding as the hydroxyl groups prefer to form hydrogen bonds in PANI. Overall, main peaks of PANI at around 2889.9, 1663, 1505.8, and 1293.7 $cm^{-1}$ were exhibited in all PANI/G composite

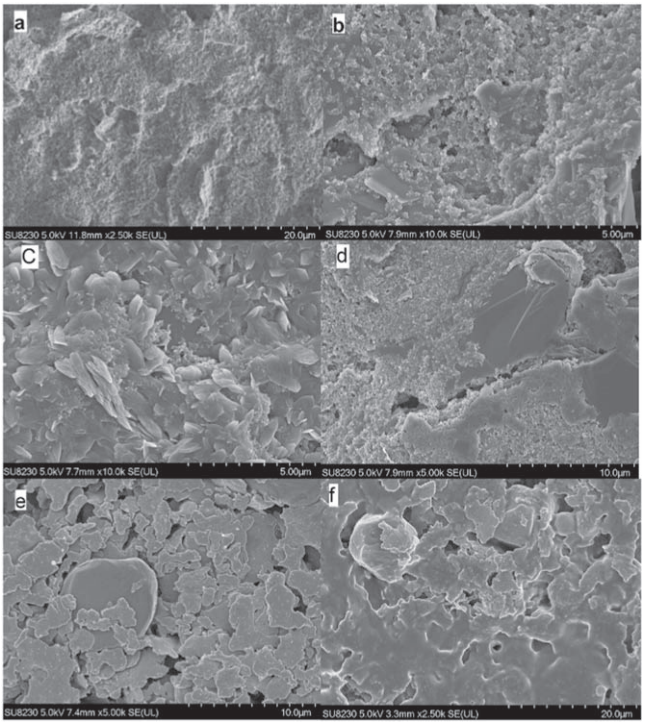


**Figure 2.** SEM images of printed PANI/G composite samples with different graphite loading: (a) graphite, (b) PANI/G 1, (c) PANI/G 2, (d) PANI/G 3, (e) Ag/AgCl, and (f) PANI/G on Ag/AgCl.

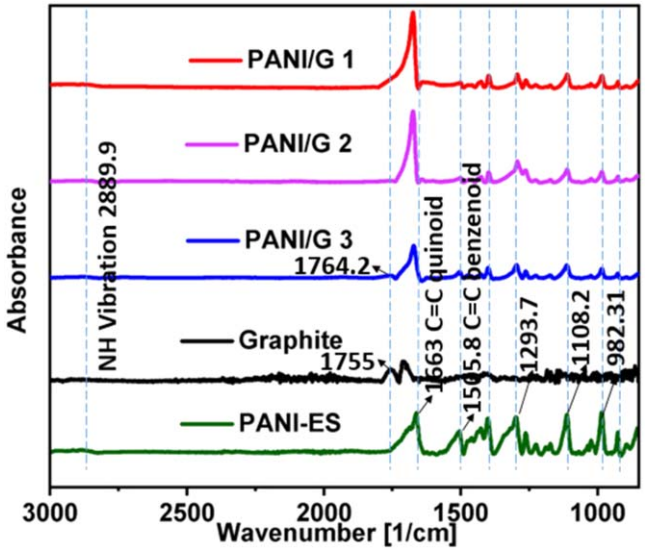


**Figure 3.** FTIR spectra of graphite (G), polyaniline (PANI), PANI/G 1, PANI/G 2, PANI/G 3.

samples. The main peak of graphite at 1755 $cm^{-1}$ appeared in the PANI/G 3 composite with a peak shift to the 1764.2 $cm^{-1}$. The peaks are shifted from 1108.2 to 1110 $cm^{-1}$ in PANI/G 1, PANI/G 2, and in PANI/G 3 the peak shifted to 1113.2 $cm^{-1}$. The shift of the peak at the C=N region is due to the lower electron delocalization after de-doping of the PANI chain.[31] The main reason of the peak shifts is due to the interlayer bonding between graphite and PANI. The intercalation between PANI and graphite lead to weaker N–H bonding as the hydroxyl group prefers to form the hydrogen bond in PANI; which is the reason of less intercalation among PANI and graphite.

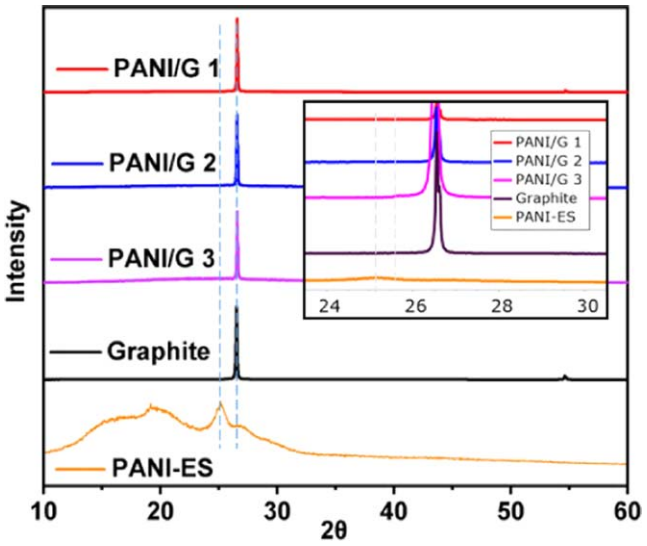


**Figure 4.** XRD pattern of Polyaniline (PANI), Graphite (G), PANI/G 1, PANI/G 2 and PANI/G 3.

**Table I. The formulation of PANI/G composites at different weight percent of graphite.**

| Samples | Weight percent of graphite content (wt%) |
|---|---|
| PANI-ES | 0 |
| Graphite | 100 |
| PANI/G 1 | 20 |
| PANI/G 2 | 50 |
| PANI/G 3 | 80 |

The polyaniline chains were anchored by the graphite particles, which resulted in further electron displacement. This explanation was also consistent with the XRD results. Intensities of PANI/G composites were different at the peak around 3000 $cm^{-1}$. This is attributed to presence of the hydroxyl group in graphite and N–H bonding in polyaniline, respectively. The intensities of PANI/G 3 composite are more than PANI/G 1 and PANI/G 2 in this region which indicate that PANI and graphite were successfully synthesized.

*XRD diffractogram.*—X-ray diffraction (XRD) patterns presented in Fig. 4 provides an insight into the effect of PANI on the graphite crystal structure. The peak shown by PANI was observed at $2\theta = 25.15°$ which corresponded to the (200) plane having orthorhombic structure. In graphite pattern, a sharp peak was observed at $2\theta = 26.58°$. A similar peak has been observed in all forms of carbon composites.[48] The peak of graphite has been observed in all three PANI/G composites and, as the graphite ratio increased in the composites to 80 wt% in PANI/G 3, the peak of polyaniline also appeared at $2\theta = 25.8°$.

The increase in intensity of the graphite peak at approximately 26°–27° in the composites shows that the graphite structure became more crystalline which is referred as the graphite plane. This structure change is due to the charge transfer between the PANI and graphite crystallites, which result in a higher degree of structural ordering in the normal direction to the graphene planes as the atomic positions within the graphene planes become more relaxed.[49] PANI/G 1 exhibited a broad diffraction peak at $2\theta = 26.55°$ suggesting that the composites started to change from partial amorphous to crystalline form by increasing the amount of graphite into the PANI structure by solution method. The peaks slowly shifted to $2\theta = 26.57°$ in PANI/G 3 as the amount of graphite increased.

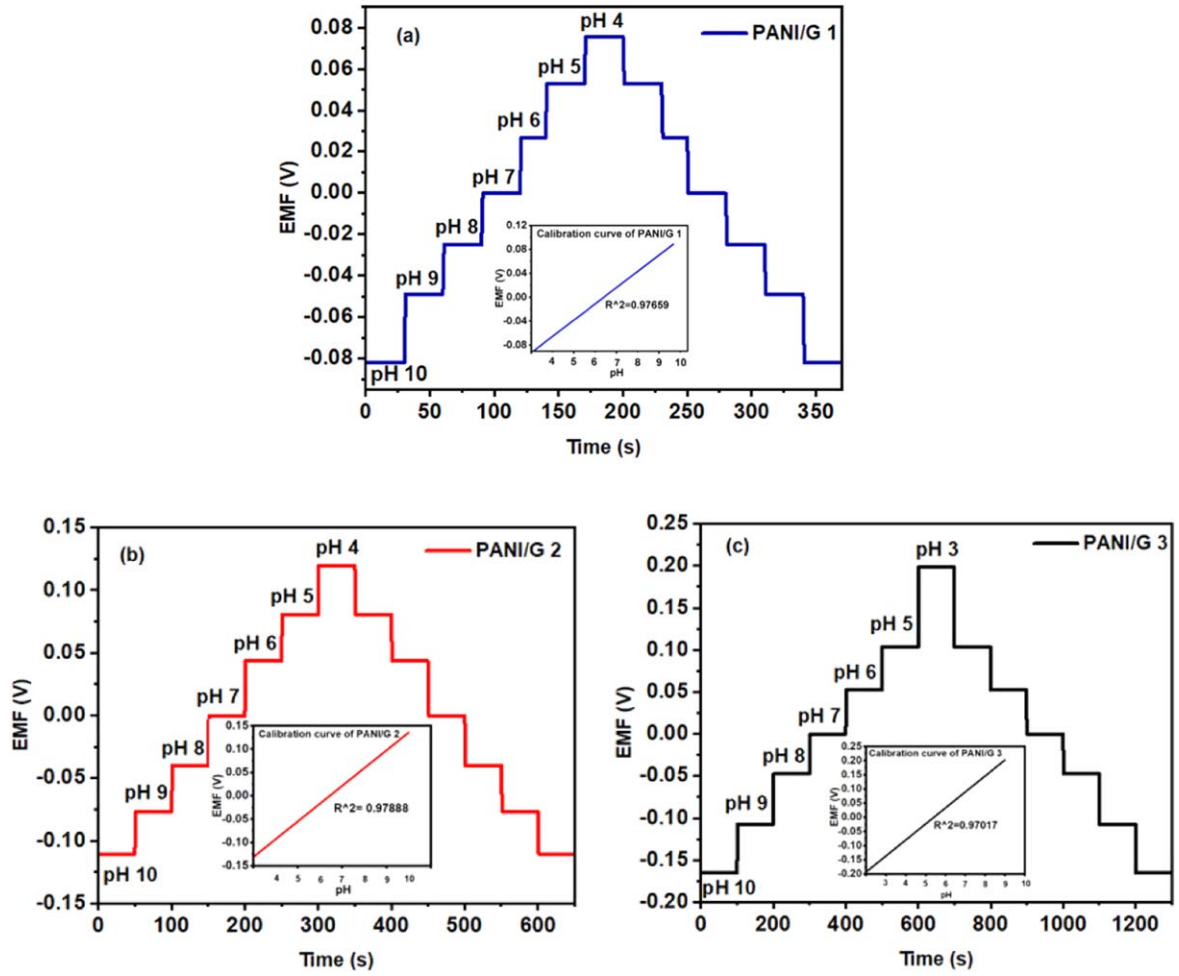


**Figure 5.** Sensitivity test for pH from the sensors fabricated from (a) PANI/G 1, (b) PANI/G 2 and (c) PANI/G 3 composites in the pH range from 3 to 10.

***pH sensors results and discussion.***—Both pH sensitivity and stability were different in sensors with a screen-printed graphite layer modified with PANI/G 1, PANI/G 2 and PANI/G 3. The sensors functionality improved as the ratio of graphite increased in the composites. The EMF measurement between the working electrode and the Ag/AgCl reference electrode provides electrochemical characteristics of the potentiometric pH sensor. The EMF values were measured by immersing the pH sensors in various pH levels solutions ranging from 3 to 10 (Fig. 5). When immersing the sensors in the buffer solutions, EMF signals changed with varying pH values and reached a steady-state point. EMF measurement results were collected and reported when steady-state was reached. The stability duration was also reported as the duration of which the voltage remained stable.

Initial tests have been done using graphite and PANI individually as the WE. Without any PANI, graphite did not show any reaction to pH changes. Applying PANI on a graphite film as the WE resulted in a response to pH changes with an average sensitivity of 50 mV $pH^{-1}$ but with a stability of 30 s in each solution, which is less than the stability when using the PANI/G 3 nanocomposite printed on graphite as the WE. The sensors modified with PANI/G 1 composite exhibited 25 mV $pH^{-1}$ sensitivity and a stability of 30 s when tested in different pH levels with various cycles. The sensors modified with PANI/G 2 composite exhibited a better sensitivity and stability of 40 mV $pH^{-1}$ and 50 s, respectively. The sensors modified with PANI/G 3 composite reached a near-Nernstian sensitivity of 53 mV $pH^{-1}$ and about 2 min stability (Fig. 6a). As graphite concentration increased from PANI/G 1 to PANI/G 3 samples, the sheet resistance of the dried films decreased from 553 kΩ to 17.5 kΩ. The percolation threshold was found to be approximately 75% of graphite. PANI/G 3 being the most conductive nanocomposite showed the most sensitivity and stability in pH sensing.

The PANI/G 3 composite which exhibited the most promising result was then deposited on Ag/AgCl electrode without the graphite layer to investigate its role in sensitivity and stability of the sensor. The sensors modified with PANI/G 3 composite on Ag/AgCl electrode without the graphite layer showed the sensitivity of about 33 mV $pH^{-1}$ (Fig. 6b) and it showed a good repeatability (Fig. 7). The response time of the sensor fabricated with all three compositions was fast and on average at 15 s, but the stability was much lower than the sensors with the graphite layer which could be due to the insufficient active sites on the surface of Ag/AgCl film for successful attachment of the PANI chain in compare to graphite film as showed in SEM characterization.

The sensor fabricated from PANI/G 3 composite has been characterized for repeatability and selectivity. The sensor has been immersed in different acidic and alkaline solutions with slight pH difference in multiple cycles without cleaning the sensor and giving time in every solution to reach the stability point. The sensor was in environment after immersing in every solution for 1–2 s to monitor the voltage decrease time.

One of the most important factors for potentiometric pH sensors is the selectively to measure $H_3O^+$ ion in the presence of other interfering ions. In this study, we selected some of the ions in that are present in blood as they are important in preventing blood cells and can interfere with $H_3O^+$ ion while measuring the pH. Separate-solution method (SSM) has been used to evaluate selectivity coefficients of pH sensors against different interfering ions of $K^+$,

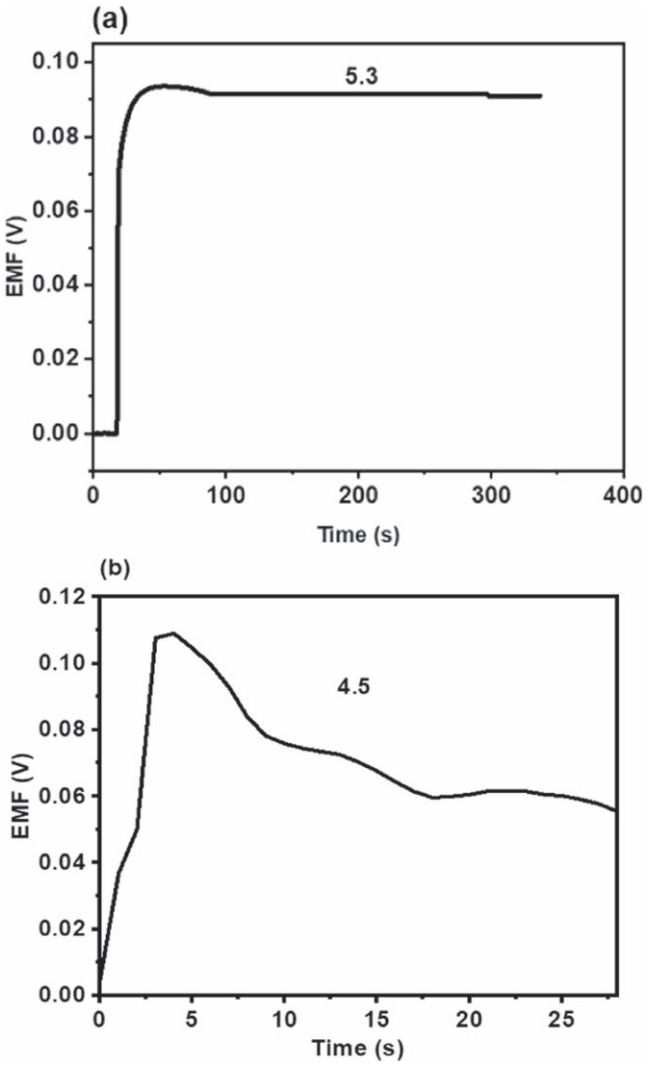


**Figure 6.** Stability and response time test for (a) the sensor modified with PANI/G 3 composite printed on the graphite layer and (b) the sensor modified with PANI/G 3 composite printed directly on Ag/AgCl electrode without graphite layer.

**Table II. Selective coefficients of pH sensors using SSM for primary ion ($H^+$) against interfering ions.**

| Ions | $\log K^{POT}_{AB}$ | $K^{POT}_{AB}$ |
|---|---|---|
| $K^+$ | −8.61 | $2.46 \times 10^{-9}$ |
| $Na^+$ | −8.50 | $3.15 \times 10^{-9}$ |
| $Ca^{2+}$ | −9.03 | $9.41 \times 10^{-10}$ |
| $Zn^+$ | −9.04 | $9.03 \times 10^{-10}$ |
| $[PO_4]^{3-}$ | −9.81 | $1.55 \times 10^{-10}$ |

$Na^+$, $Ca^{2+}$, $Zn^+$ and $[PO_4]^{3-}$. The EMF responses were measured in different solutions containing every ion at a same concentration of 3 M. The selectivity coefficient ($K_{AB}^{POT}$) in SSM can be calculated as follows:[50,51]

$$\log K_{AB}^{POT} = \frac{(E_B - E_A)Z_A F}{2.303RT} + \left(1 - \frac{Z_A}{Z_B}\right)\log a_A \qquad [2]$$

where $K_{AB}^{POT}$ is the potentiometric selectivity coefficient for ion B with respect to the primary ion A, E is the experimentally determined galvanic potential difference of ISE cell (in V), R is the gas constant equal to 8.314510 J $K^{-1}mol^{-1}$, T is the absolute temperature in K, F is the Faraday constant, $9.6485309 \times 10^4$ C $mol^{-1}$, $a_A$ is the activity of ion A and Z is the charge number of every ion. The measured K values of pH sensor fabricated with PANI/G 3 composite are shown in Table II. All of the K values for pH sensor are below $10^{-9}$ which indicates that the pH sensor can accurately measure $H^+$ over interfering ions.

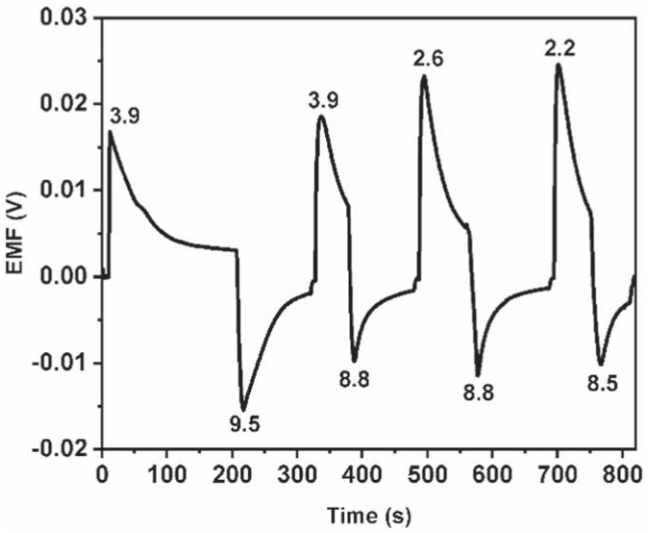


**Figure 7.** Repeatability of the sensor modified with PANI/G 3 composite.

## Conclusions

We fabricated a two electrode potentiometric pH sensor by screen-printing Ag/AgCl as the reference electrode and a graphite layer as working electrode. We then modified the working electrode with PANI/G composites using aerosol-jet printing which is more flexible in terms of the range of viscosity of the materials that can be printed. PANI/G nanocomposites have been characterized to investigate the effect of graphite loading in active nanocomposites on sensitivity and stability of the sensors. As potentiometry is a robust technique, sensors fabricated with all nanocompositions had a fast response time of 15 s and as the graphite loading increased, the functionality of the sensor in terms sensitivity and stability improved. The sensors modified with PANI/G 3 exhibited a sensitivity of 53 mV $pH^{-1}$ and exhibited good repeatability and selectivity.

## Acknowledgments

The authors would like to express their appreciation for all the financial support from the Regroupement Stratégique en Microsystèmes du Québec (ReSMiQ) and the NSERC Green Electronics Network (GreEN). We would also like to acknowledge the LACIME (Laboratoire de communications et d'intégration de la microélectronique) and the research centers of NanoQAM (Centre de Recherche sur les Nanomateriaux et l'Énergie).

## ORCID

Shirin Mahinnezhad https://orcid.org/0000-0002-6803-0025

## References

1. C. U. Seo et al., *J. Ind. Eng. Chem.*, **64**, 97 (2018).
2. A. Scott et al., *ECS Sens. Plus*, **1**, 014601 (2022).
3. F. D. S. Santos et al., *ECS Sens. Plus*, **1**, 013603 (2022).
4. T. R. Ray et al., *Chem. Rev.*, **119**, 5461 (2019).
5. R.-I. Stefan-van Staden, *ECS Sens. Plus*, **1**, 011603 (2022).
6. V. Chaudhary, A. K. Kaushik, H. Furukawa, and A. Khosla, *ECS Sens. Plus*, **1**, 013601 (2022).
7. S. Singh, J. Wang, and S. Cinti, *ECS Sens. Plus*, **1**, 023401 (2022).
8. U.-W. Grummt, A. Pron, M. Zagorska, and S. Lefrant, *Anal. Chim. Acta*, **357**, 253 (1997).

9. H. Varela, R. M. Torresi, and D. A. Buttry, *J. Braz. Chem. Soc.*, **11**, 32 (2000).
10. K. Qu, M. Fang, S. Zhang, H. Liu, and X. Zeng, *Polymers*, **10**, 1191 (2018).
11. S. N. Alam, N. Sharma, B. C. Ray, S. Yadav, and K. Biswas, *Ceram. Int.*, **43**, 11376 (2017).
12. S. Namilae, J. Li, and S. Chava, *Mech. Adv. Mater. Struct.*, **26**, 1333 (2019).
13. D. Bychanok et al., *J. Phys. Appl. Phys.*, **51**, 145307 (2018).
14. H. Fukushima, L. T. Drzal, B. P. Rook, and M. J. Rich, *J. Therm. Anal. Calorim.*, **85**, 235 (2006).
15. T. T. T. Toan, *ECS Sens. Plus*, **1**, 031603 (2022).
16. R. Sharma, G. Lakshmi, A. Kumar, and P. Solanki, *ECS Sens. Plus*, **1**, 010603 (2022).
17. E. Bilbao et al., *Sens. Actuators B Chem.*, **346**, 130558 (2021).
18. T. Guinovart, G. Valdés-Ramírez, J. R. Windmiller, F. J. Andrade, and J. Wang, *Electroanalysis*, **26**, 1345 (2014).
19. K. Crowley, M. R. Smyth, A. J. Killard, and A. Morrin, *Chem. Pap.*, **67**, 771 (2013).
20. T. N. Atiqah et al., *Polym. Bull.*, **75**, 209 (2018).
21. I. Y. Sapurina and M. A. Shishov, *New Polym. Spec. Appl.*, **740**, 272 (2012).
22. G. Wang, W. Xing, and S. Zhuo, *Electrochim. Acta*, **66**, 151 (2012).
23. B. D. Gupta and D. K. Sharma, *Opt. Commun.*, **140**, 32 (1997).
24. B. Adhikari and S. Majumdar, *Prog. Polym. Sci.*, **29**, 699 (2004).
25. J. Qi, X. Xu, X. Liu, and K. T. Lau, *Sens. Actuators B Chem.*, **202**, 732 (2014).
26. N. B. Clark and L. J. Maher, *React. Funct. Polym.*, **69**, 594 (2009).
27. T. Alizadeh and L. H. Soltani, *J. Hazard. Mater.*, **248**, 401 (2013).
28. Z. Ihdene et al., *Sens. Actuators B Chem.*, **203**, 647 (2014).
29. J.-S. Kim, S.-O. Sohn, and J.-S. Huh, *Sens. Actuators B Chem.*, **108**, 409 (2005).
30. M. M. Nobrega, C. M. Izumi, and M. L. Temperini, *Polym. Degrad. Stab.*, **113**, 66 (2015).
31. L. Yu et al., *Compos. Part Appl. Sci. Manuf.*, **43**, 2039 (2012).
32. N. H. Ho, D. L. Glasco, and J. G. Bell, *ECS Sens. Plus*, **1**, 020601 (2022).
33. S. K. Das, K. K. Nayak, P. R. Krishnaswamy, V. Kumar, and N. Bhat, *ECS Sens. Plus* (2022).
34. M. Yang and K. Choy, *Mater. Lett.*, **288**, 129335 (2021).
35. S. G. Pawar, M. A. Chougule, S. Sen, and V. B. Patil, *J. Appl. Polym. Sci.*, **125**, 1418 (2012).
36. D. J. Boday, B. Muriithi, R. J. Stover, and D. A. Loy, *J. Non-Cryst. Solids*, **358**, 1575 (2012).
37. J. H. Li, M. Li, Q. Liu, and H. F. Da, *J. Mater. Sci., Mater. Electron.*, **22**, 1016 (2011).
38. C. Sun et al., *Appl. Energy*, **282**, 116041 (2021).
39. R. L. McCreery, *Chem. Rev.*, **108**, 2646 (2008).
40. C. Xiang et al., *Mater. Lett.*, **64**, 1313 (2010).
41. J.-L. Zeng et al., *Appl. Energy*, **115**, 603 (2014).
42. S. E. Bourdo and T. Viswanathan, *Carbon*, **43**, 2983 (2005).
43. L. Dai, *Intelligent Macromolecules For Smart Devices: From Materials Synthesis To Device Applications* (Berlin)(Springer Science & Business Media) (2004).
44. M. Diantoro, M. Z. Masrul, and A. Taufiq, *J. Phys.: Conf. Ser.*, **1011**, 012065 (2018), IOP Publishing.
45. K. Kakde, *Indian J. Sci. Technol.*, **10**, 20 (2017).
46. E. R. Holland, S. J. Pomfret, P. N. Adams, and A. P. Monkman, *J. Phys. Condens. Matter*, **8**, 2991 (1996).
47. S. Ameen, G. Lakshmi, and M. Husain, *J. Phys. Appl. Phys.*, **42**, 105104 (2009).
48. E. M. Elnaggar, K. I. Kabel, A. A. Farag, and A. G. Al-Gamal, *J. Nanostructure Chem.*, **7**, 75 (2017).
49. T. N. Atiqah, S. J. Tan, K. L. Foo, A. G. Supri, and M. F. Abdullah, *Mater Sci. Forum*, **889**, 9 (2017), Trans Tech Publ.
50. J. H. Yoon et al., *J. Colloid Interface Sci.*, **490**, 53 (2017).
51. J. Hu, A. Stein, and P. Bühlmann, *TrAC, Trends Anal. Chem.*, **76**, 102 (2016).